PERGAMON

International Journal of Heat and Mass Transfer 43 (2000) 3275–3285

International Journal of HEAT and MASS TRANSFER

www.elsevier.com/locate/ijhmt

Radiative transfer in arbitrarily-shaped axisymmetric enclosures with anisotropic scattering media

Edmundo M. Nunes[a], Vijay Modi[a], Mohammad H.N. Naraghi[b,*]

[a]*Department of Mechanical Engineering, Columbia University, New York, NY 10029, USA*
[b]*Department of Mechanical Engineering, Manhattan College, Riverdale, NY 10471, USA*

Received 4 June 1999; received in revised form 3 December 1999

Abstract

Two numerical models for solving thermal radiative transport in irregularly-shaped axisymmetric bodies containing a homogeneous, anisotropically scattering medium are presented. The *N*-bounce method approximates total exchange factors by summing direct and user-designated higher order terms representative of multiple reflections/scattering. The source function approach is an intensity-based method relating the source function (gas leaving intensity) to the surface leaving intensity. Both methods are based on the Discrete Exchange Factor method, where exchange factors between arbitrarily-oriented differential surface and/or volume elements are calculated in a straightforward approach. The present methods are capable of addressing blockage effects produced by inner and/or outer blocking bodies. The results obtained via the current methods are found to be in good agreement with the existing solutions to several axisymmetric benchmark problems. The solutions to several two-dimensional axisymmetric problems are presented.

1. Introduction

The numerous technological advancements achieved within the past two decades are fueling industrial efforts to push the envelopes of product yield and quality. Complex materials processes, such as the Czochralski (CZ) crystal growth, vertical Bridgmann crystal growth, and optical fiber drawing processes, are numerically simulated for purposes of process optimization and promoting insight into extraneous thermophysical issues. Radiative heat transport plays a vital role in these material processes, as well as other engineering processes, including glass manufacturing, rocket-nozzle analysis, and combustion chamber design. Radiative analyses of these axisymmetric systems are, however, generally simplified or often neglected, due to the intrinsic difficulties associated with making detailed radiation calculations. A few of the inherent radiative complexities encountered in these systems include consideration of the arbitrary shape of the enclosure, shadowing effects produced by inner/outer blocking bodies, and anisotropically scattering media. Nunes and Naraghi [1] have addressed these concerns for isotropically scattering media by generalizing Modest's [2] view factor scheme using the Discrete Exchange Factor (DEF) [3] formulation. Thus, the motivation of this work is to extend Nunes and Naraghi's [1] DEF-based model for systematically

* Corresponding author. Tel.: +1-718-862-7367; fax: +1-718-862-7163.

E-mail addresses: emn17@columbia.edu (E.M. Nunes), modi@columbia.edu (V. Modi), mnaraghi@manhattan.edu (M.H.N. Naraghi).

0017-9310/00/$ - see front matter
PII: S0017-9310(99)00384-1

Nomenclature

a	degree of anisotropy in Eq. (24)
a_j	absorptance of node j
$\overline{ds_i s_j}$	direct exchange factor between surface ring elements i and j
$\overline{ds_i s_{jk}}$	direct exchange factor between a point on surface ring element i and element k on surface ring element j
$\overline{ds_i v_j}$	direct exchange factor between surface ring element i and volume ring element j
$\overline{ds_i v_{jk}}$	direct exchange factor between a point on surface ring element i and element k on volume ring element j
$\overline{dv_i s_j}$	direct exchange factor between volume ring element i and surface ring element j
$\overline{dv_i s_{jk}}$	direct exchange factor between a point on volume ring element i and element k on surface ring element j
$\overline{dv_i v_j}$	direct exchange factor between volume ring elements i and j
$\overline{dv_i v_{jk}}$	direct exchange factor between a point on volume ring element i and element k on volume ring element j
$\overline{dz_i z_j}$	unified direct exchange factor between ring elements i and j
$\overline{DZ_i Z_j}$	unified total exchange factor between ring elements i and j
E	emissive power
I_{s_i}	surface leaving intensity from node i
$I_{v_{i,j}}$	intensity leaving volume node i directed towards node j
K_t	extinction coefficient
N_{ce}	number of circumferential elements
N_{sre}	number of surface ring elements
N_{vre}	number of volume ring elements
q''	radiative heat flux
q'''	radiative heat source
$\mathbf{r}$	position vector
r	radial coordinate
$r_{i,k,j}$	reflectance of element k
T	temperature
w	numerical integration weight factor
z	axial coordinate

Greek symbols

ϵ	emissivity
ϕ_i, ϕ_j	function defined by Eq. (7)
$\Phi_{i,k,j}$	scattering phase function
θ	tilt angle of surface with respect to z-axis
ψ	azimuth angle
ρ	reflectivity
σ	Stefan–Boltzmann constant = 5.67051 × 10^{-8} W/(m^2 K^4)
ω_o	scattering albedo

Subscripts

i	designates emitting ring element
j	designates receiving ring element
k_1, k_2	designates reflecting/scattering element
max	designates maximum
min	designates minimum
s	designates surface
v	designates volume
w	designates wall

computing radiative transfer in axisymmetric enclosures to include the effects of anisotropic scattering.

Investigators have, in previous works, implemented various numerical methods for solving the radiative transfer equation (RTE) for specific axisymmetric geometries. Kaminski [4] utilized the P_1 differential approximation and Monte Carlo methods for solving radiative transfer in a gray, truncated cone. Yin and Jaluria [5] modeled the radiative exchange of heat between an optical fiber furnace and preform during neck-down using the zonal method. In a recent work by Kim and Baek [6], benchmark results are presented for a nozzle-shaped cylindrical enclosure using several techniques, including a hybrid method of a modified discrete ordinates method (MDOM) for body-fitted axisymmetric geometries, a three-dimensional finite volume method (FVM), and an axisymmetric FVM. All these analyses, however, neglect the effects of volumetric scattering. In fact, a review of the existing literature indicates that radiative analyses of axisymmetric media with anisotropic scattering is limited to circular cylindrical geometries. Stockham and Love [7] employed the Monte Carlo method to investigate the radiative transfer to the exterior base region of a finite cylindrical dispersion of absorbing, emitting, and anisotropically scattering particles. Azad and Modest [8] reported heat flux results for an infinitely long gray cylinder using an exact formulation derived explicitly for linear anisotropic scattering. Additionally, they presented modified differential and exponential kernel approximations for linear anistropically scattering media. Thynell [9] used the RTE, cast in an integral form of the Fredholm type, for absorbing, emitting, and linear-anisotropically scattering media, to compute the spectral hemispherical and hemispherical plume emissivities of a one-dimensional cylinder. Cros-

bie and Dougherty [10] presented an exact solution to radiative transfer in a finite cylinder with anisotropic scattering, with the resulting expressions for the source function, heat flux, and intensity given in integral form. In an effort to decouple the transfer equation from the energy equation, this formulation, however, neglects the effects of emission. Thus, to the authors' knowledge, a numerical model which incorporates geometrical, as well as optical complexity, such as anisotropic scattering, for finite axisymmetric systems, is inexistant to date.

Two numerical models based on the N-bounce [11] and source function [12] variations of the DEF method, are applied to Nunes and Naraghi's [1] exchange factor model in order to address the aforementioned concerns. In the N-bounce method, total exchange factors between emitting/receiving elements are computed by summing direct radiative and N higher order transfer terms, representing multiple reflections/scattering or bounces among enclosing surfaces/media. The source function approach is based on simultaneously solving two integral equations relating the volumetric source function and surface leaving intensity, using discrete exchange factors in place of solid angle discretization. The source function approach is extremely versatile and insensitive to the type and degree of scattering in its solution procedure. Several benchmark problems are solved, including radiative transfer in a truncated cone, nozzle-shaped cone and a one-dimensional cylinder, to verify the presented methods.

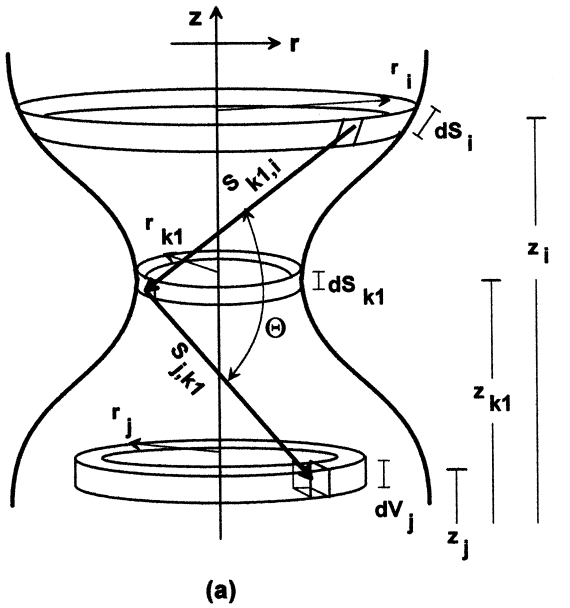

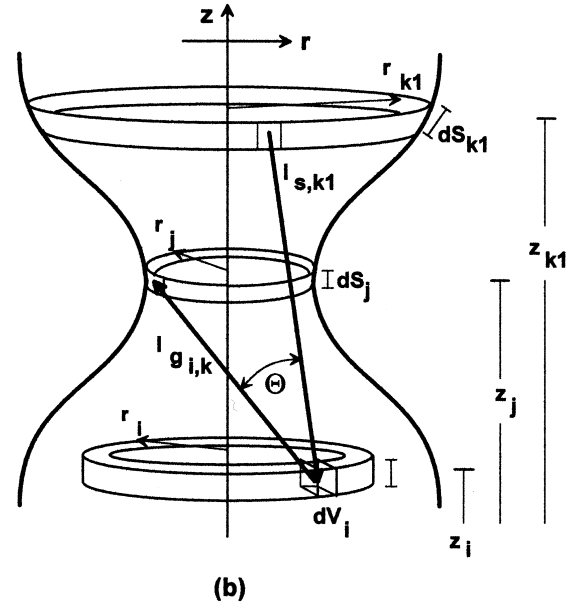

Fig. 1. (a) Two-dimensional view of an axisymmetric body used in N-bounce formulation; (b) two-dimensional view of an axisymmetric body used in source function formulation

2. Mathematical formulation

2.1. N-bounce method

Consider the axisymmetric enclosure shown in Fig. 1(a). The enclosure is comprised of arbitrarily-shaped inner and outer surfaces. All surfaces are diffuse and gray; the medium is homogeneous and anisotropically scattering. The computation of radiative transfer from position vector $\mathbf{r}_i$ to $\mathbf{r}_j$ is complicated by the presence of directional-biased scattering and shadowing/blockage effects, ensuing from the geometric configuration of the enclosure. The N-bounce method asserts that the total exchange of radiant heat from position vector $\mathbf{r}_i$ to $\mathbf{r}_j$ can be obtained by summing a user-defined N number of bounce terms, representative of the maximum number of scattering/reflections which a radiative beam undergoes, before reaching $\mathbf{r}_j$. The unified total exchange factor expression [11] in discretized form for the zero-, one-, and two-bounce approximations can be expressed as:

$$\overline{D_i Z_i Z_j} = \overline{dz_i z_j} \tag{1}$$

$$\overline{DZ_iZ_j} = \overline{dz_iz_j}a_j + \sum_{k_1=1}^{N_{sre}+N_{vre}} \overline{dz_iz_{k_1}} r_{i,\,k_1,\,j} w_{k_1} \overline{dz_{k_1}z_j} \tag{2}$$

$$\overline{DZ_iZ_j} = \overline{dz_iz_j}a_j + \sum_{k_1=1}^{N_{sre}+N_{vre}} \overline{dz_iz_{k_1}} r_{i,\,k_1,\,j} w_{k_1} \overline{dz_{k_1}z_j} + \sum_{k_1=1}^{N_{sre}+N_{vre}} \times \sum_{k_2=1}^{N_{sre}+N_{vre}} \overline{dz_iz_{k_1}} r_{i,\,k_1,\,k_2} w_{k_1} \overline{dz_{k_1}z_{k_2}} r_{k_1,\,k_2,\,j} w_{k_2} \overline{dz_{k_2}z_j} \tag{3}$$

where N_{sre} denotes the total number of surface ring elements; N_{vre} denotes the total number of volume ring elements, and the term $\overline{dz_iz_j}$ is the unified direct exchange factor between position nodes i and j. If nodes i and j are located on any enclosure surface, then $\overline{dz_iz_j}$ is a surface-to-surface direct exchange factor, given by $\overline{ds_is_j}$. The remaining direct exchange factors, $\overline{ds_iv_j}$, $\overline{dv_is_j}$, and $\overline{dv_iv_j}$, are defined within $\overline{dz_iz_j}$ in a similar way. The unified total exchange factor expression, $\overline{dZ_iZ_j}$ is defined in the same manner. The reflectance, $r_{i,\,k_1,\,j}$, of differential element k_1 is defined as the reflectivity, ρ, for surface elements and the scattering albedo-phase function product, $\omega_0\Phi_{i,\,k_1,\,j}$, for the anisotropically scattering medium. The absorptance, a_j of surface node j is the absorptivity of the surface, where, for volume node j, the absorptance is $1-\omega_0$. It is important to note that the absorptance of the last terms of Eqs. (1)–(3) is equivalent to one, so as to satisfy the energy conservation law. The term, w_k denotes the numerical integration weight factors for surface elements (w_s) and volume elements (w_v). It should be noted that the original N-bounce approach [11] is only applicable to three-dimensional configurations. Since the geometric configuration of the enclosure is axisymmetric, the direct exchange factors can be conveniently computed between concentric differential ring elements using the method outlined in [1]. The unified direct exchange factor expression, based on symmetry with respect to the azimuthal angle, is given below.

$$\overline{dzz}(\mathbf{r}_i,\,\mathbf{r}_j) = \times \frac{(-2)^{(b_i+b_j)} K_t^{(1-b_j)} r_i^{b_j} r_j^{(b_i+1)} \cos^{b_i}(\theta_i)\cos^{b_j}(\theta_j) w_j}{4^{(1-b_i)}\pi} \times \int_{\psi_{min}^{i,\,j}}^{\psi_{max}^{i,\,j}} \frac{\left(\phi_i - \cos(\psi_{i,\,j})\right)^{b_i}\left(\phi_j - \cos(\psi_{i,\,j})\right)^{b_j} e^{-K_t|r_i - r_j|}}{|\mathbf{r}_i - \mathbf{r}_j|^{(b_i+b_j+2)}} \times d\psi_{i,\,j} \tag{4}$$

or, in discretized form:

$$\overline{dz_iz_j} = \frac{(-2)^{(b_i+b_j)} K_t^{(1-b_j)} r_i^{b_j} r_j^{(b_i+1)} \cos^{b_i}(\theta_i)\cos^{b_j}(\theta_j)}{4^{(1-b_i)}\pi} \times \sum_{k=1}^{N_{ce,\,j}} \frac{\left(\phi_i - \cos(\psi_{i,\,j^k})\right)^{b_i}\left(\phi_j - \cos(\psi_{i,\,j^k})\right)^{b_j} e^{-K_t|r_i - r_{j^k}|}}{|\mathbf{r}_i - \mathbf{r}_{j^k}|^{(b_i+b_j+2)}} w_{j^k} \tag{5}$$

where

$$|\mathbf{r}_i - \mathbf{r}_j|^2 = r_i^2 + r_j^2 - 2r_ir_j\cos\psi + (z_j - z_i)^2 \tag{6}$$

$$\phi_i = \frac{r_i}{r_j} + \frac{z_j - z_i}{r_j}\tan\theta_i, \qquad \phi_j = \frac{r_j}{r_i} + \frac{z_i - z_j}{r_i}\tan\theta_j \tag{7}$$

where, for differential ring element i, $b_i = 1$ for a surface element; $b_i = 0$ for a volume element, and for ring element j, $b_j = 1$ for a surface element; $b_j = 0$ for a volume element. The azimuthal angles ψ_{min} and ψ_{max} represent the limiting angles from which a reference point (at $\psi = 0$) on an emitting ring element i can see a receiving ring element j. The values of ψ_{min} and ψ_{max} are governed by the orientation of surface elements relative to the surface/volume ring elements to/from which radiative energy is being transferred and the presence of inner/outer blocking bodies (see [1]).

The main difficulty presented by integrating the unified direct exchange factor expression into the one- or two-bounce equations, given by Eqs. (2) and (3), is in computing the phase function, Φ. This is primarily due to the use of azimuthal symmetry in formulating the unified direct exchange factor equation. In an effort to clarify these statements, consider the three ring el-

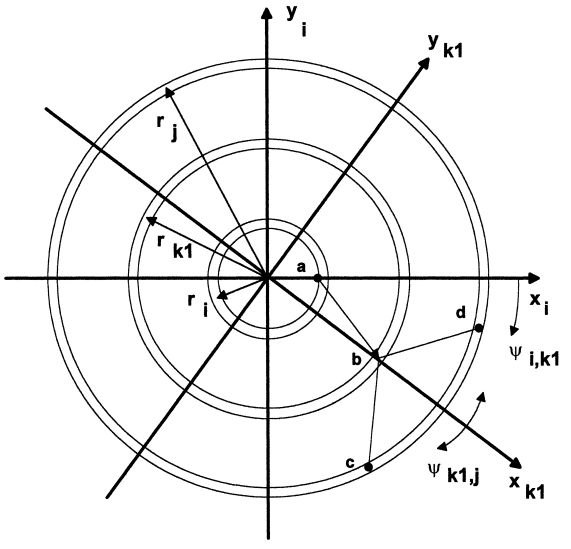

Fig. 2. Two-dimensional view of ring elements in r–ψ plane depicting scattering at point b on ring element k_1.

ements shown in the r–ψ or x–y plane in Fig. 2. Elements i, k_1, and j are emitting, reflecting/scattering, and receiving ring elements. Point a is a reference point (at $\psi_{i,\,k_1}=0$), situated on the x_i-axis, which emits radiation in the direction heading to point b on ring element k_1. With the radiative beam now at ring element k_1, point b becomes a reference point (at $\psi_{k_1,\,j}=0$), situated on the x_{k_1}-axis, which scatters the radiative beam into the direction of point c, as well as its symmetric counterpart, point d. Clearly, scattering angles abc and abd are not equal, giving two different values for the phase function at point b. This disparity can be easily resolved by using the average of the phase function, all the while retaining the basis of azimuthal symmetry in the definition of the direct exchange factor expression, i.e.:

$$\bar{\Phi}_{a,\,b,\,c}=\frac{\Phi_{a,\,b,\,c}+\Phi_{a,\,b,\,d}}{2} \tag{8}$$

It is very important that the multiple bounce exchange factors satisfy the conservation of energy equations, namely:

$$\sum_{j=1}^{N_{\mathrm{sre}}}\overline{ds_i s_j}w_{\mathrm{s}_j}+\sum_{j=1}^{N_{\mathrm{vre}}}\overline{ds_i v_j}w_{\mathrm{v}_j}=1 \tag{9}$$

$$\sum_{j=1}^{N_{\mathrm{sre}}}\overline{dv_i s_j}w_{\mathrm{s}_j}+\sum_{j=1}^{N_{\mathrm{vre}}}\overline{dv_i v_j}w_{\mathrm{v}_j}=1 \tag{10}$$

Since the exchange factors are evaluated numerically, normalization of the exchange factors is required. The zero-bounce or direct exchange factors are normalized by invoking an error minimization process based on a least squares smoothing technique using Lagrangian multipliers [13]. Each of the terms of the one-bounce exchange factors are normalized, making it a two-step normalization procedure. The first term is normalized just as a direct exchange factor would be. The second term is normalized using the following equation in place of Eqs. (9) and (10) as a constraint.

$$\sum_{j=1}^{N_{\mathrm{sre}}+N_{\mathrm{vre}}}\sum_{k_1=1}^{N_{\mathrm{sre}}+N_{\mathrm{vre}}}\overline{dz_i z_{k_1}}r_{i,\,k_1,\,j}\overline{dz_{k_1} z_j}w_{k_1}w_j = 1-\sum_{j=1}^{N_{\mathrm{sre}}+N_{\mathrm{vre}}}\overline{z_i z_j}w_j a_j \tag{11}$$

where the left-hand term represents the sum of the one-bounce terms from a point on ring element i to the enclosure; the right-hand term gives the total amount of energy emitted from a point on ring element i, which is scattered/reflected after direct transmission to all the ring elements in the enclosure. The two-bounce total exchange factors are normalized using a similar procedure.

Once the total exchange factors for the zero-, one-, or two-bounce approximations have been evaluated, the radiative heat flux at each surface/volume ring element can be computed from energy balance considerations.

$$q''_{\mathrm{s}_i}=E_{\mathrm{s}_i}-\sum_{j=1}^{N_{\mathrm{sre}}}w_{\mathrm{s},\,j}\overline{DS_j S_i}E_{\mathrm{s}_j}-\sum_{j=1}^{N_{\mathrm{vre}}}w_{\mathrm{v},\,j}\overline{DV_j S_i}E_{\mathrm{v}_j} \tag{12}$$

$$q'''_{\mathrm{v}_i}=E_{\mathrm{v}_i}-\sum_{j=1}^{N_{\mathrm{sre}}}w_{\mathrm{s},\,j}\overline{DS_j V_i}E_{\mathrm{s}_j}-\sum_{j=1}^{N_{\mathrm{vre}}}w_{\mathrm{v},\,j}\overline{DV_j V_i}E_{\mathrm{v}_j} \tag{13}$$

where $E_{\mathrm{s}_j}=\epsilon_j\sigma T_j^4$ and $E_{\mathrm{v}_j}=4K_{\mathrm{t}}(1-\omega_0)\sigma T_j^4$ are equations for the emissive power of surface/volume ring elements.

2.2. Source function method

Consider an arbitrarily-shaped axisymmetric enclosure which encompasses an absorbing, emitting, and anisotropically scattering medium, as depicted in Fig. 1(b). The equations of radiative transfer, based on the source function approach, describing the radiative transfer within the enclosure are, in discretized form, given below [12].

$$I_{\mathrm{s}_i}=\epsilon_i\frac{E_{\mathrm{s}_i}}{\pi}+\rho_i\sum_{j=1}^{N_{\mathrm{s}}}w_{\mathrm{s}_j}I_{\mathrm{s}_j}\overline{ds_i s_j}+\rho_i\sum_{j=1}^{N_{\mathrm{v}}}w_{\mathrm{v}_j}I_{\mathrm{v}_{j,\,i}}\overline{ds_i v_j} \tag{14}$$

$$I_{\mathrm{v}_{i,\,j}}=\frac{E_{\mathrm{v}_i}}{4\pi K_{\mathrm{t}}}+\sum_{k=1}^{N_{\mathrm{s}}}w_{\mathrm{s}_k}I_{\mathrm{s}_k}\omega_0\Phi_{k,\,i,\,j}\overline{dv_i s_k}+\sum_{k=1}^{N_{\mathrm{v}}}w_{\mathrm{v}_k}I_{\mathrm{v}_{k,\,i}}\omega_0\Phi_{k,\,i,\,j}\overline{dv_i v_k} \tag{15}$$

$$q''_{\mathrm{s}_i}=E_{\mathrm{s}_i}-\epsilon_i\pi\sum_{j=1}^{N_{\mathrm{s}}}w_{\mathrm{s}_j}I_{\mathrm{s}_j}\overline{ds_i s_j}-\epsilon_i\pi\sum_{j=1}^{N_{\mathrm{v}}}w_{\mathrm{v}_j}I_{\mathrm{v}_{j,\,i}}\overline{ds_i v_j} \tag{16}$$

$$q'''_{\mathrm{v}_i}=E_{\mathrm{v}_i}-4\pi K_{\mathrm{t}}(1-\omega_0)\left[\sum_{j=1}^{N_{\mathrm{s}}}w_{\mathrm{s}_j}I_{\mathrm{s}_j}\overline{dv_i s_j}+\sum_{j=1}^{N_{\mathrm{v}}}w_{\mathrm{v}_j}I_{\mathrm{v}_{j,\,i}}\overline{dv_i v_j}\right] \tag{17}$$

where I_{s_i} is defined as the surface leaving intensity from a diffuse surface at node i; $I_{\mathrm{v}_{i,\,j}}$ is the source function, representing the intensity leaving volume node i

directed towards node j; E_{s_i} and E_{v_i} are the emissive powers of surface/volume node i, respectively.

The source function equations can be easily manipulated to conform to problem types with different known quantities (e.g. surface temperature/gas heat source or surface/volume temperatures known). These equations are solved iteratively for the surface leaving intensity and source function distributions, whereupon the surface heat flux, volume heat source or volume temperature quantities are computed in a straightforward procedure. In axisymmetric systems, however, these radiative quantities are invariant in the circumferential direction. Thus, the source function equations can be modified based on the principles of axisymmetry to give:

$$I_{s_i} = \epsilon_i \frac{E_{s_i}}{\pi} + \rho_i \sum_{j=1}^{N_{sre}} \sum_{k=1}^{N_{ce,\,j}} w_{s_{jk}} I_{s_j} \overline{ds_i s_{jk}} + \rho_i \sum_{j=1}^{N_{vre}} \sum_{k=1}^{N_{ce,\,j}} w_{v_j^k} I_{v_{j,\,jk}} \overline{ds_i v_{jk}} \tag{18}$$

$$I_{v_{i,\,jn}} = \frac{E_{v_i}}{4\pi K_t} + \sum_{k=1}^{N_{sre}} \sum_{m=1}^{N_{ce,\,k}} w_{s_{km}} I_{s_k} \omega_0 \Phi_{km,\,i,\,jn} dv_i s_{km} + \sum_{k=1}^{N_{vre}} \sum_{m=1}^{N_{ce,\,k}} w_{v_{km}} I_{v_{k,\,jm}} \omega_0 \Phi_{km,\,i,\,jn} dv_i v_{km} \tag{19}$$

$$q''_{s_i} = E_{s_i} - \epsilon_i \pi \sum_{j=1}^{N_{sre}} \sum_{k=1}^{N_{ce,\,j}} w_{s_{jk}} I_{s_j} \overline{ds_i s_{jk}} - \epsilon_i \pi \sum_{j=1}^{N_{vre}} \sum_{k=1}^{N_{ce,\,j}} w_{v_j^k} I_{v_{j,\,jk}} \overline{ds_i v_{jk}} \tag{20}$$

$$q'''_{v_i} = E_{v_i} - 4\pi K_t (1-\omega_0) \left[\sum_{j=1}^{N_{sre}} \sum_{k=1}^{N_{ce,\,j}} w_{s_{jk}} I_{s_j} \overline{dv_i s_{jk}} + \sum_{j=1}^{N_{vre}} \sum_{k=1}^{N_{ce,\,j}} w_{v_{jk}} I_{v_{j,\,jk}} \overline{dv_i v_{jk}} \right] \tag{21}$$

where $N_{ce,\,j}$ denotes the number of circumferential elements in ring element j; $w_{s_{jk}}$ and $w_{v_{jk}}$ denote the numerical integration weight factor associated with circumferential element k of surface/volume ring element j, respectively; $\overline{dz_i z_{jk}}$ denotes the direct exchange factor between a reference point (at $\psi = 0$) on surface/volume ring element i and circumferential element k of surface/volume ring element j; and $I_{v_{i,\,jk}}$ denotes the source function, giving the intensity of radiation leaving a reference point (at $\psi = 0$) on volume ring element i in the direction of circumferential element k of surface/volume ring element j.

The direct exchange factor expressions found in Eqs. (18)–(21) are taken from the integrand of the unified direct exchange factor equation (4). The formulation of the axisymmetric source function equations is contingent upon equating the number of subdivisions (or circumferential elements) of two ring elements constituting a ring element pair (i.e. the number of subdivisions in ring elements i and j are equivalent when both ring elements are transferring radiation). This allows the following condition to be valid:

$$I_{v_{jk,\,i}} = I_{v_{j,\,ik}} \tag{22}$$

When implemented into code, the notation of the expression on the right side of Eq. (22) reduces computer storage and substantially improves computational time. Again, one must be careful when computing the phase function during the solution prcoess, due to the imposed azimuthal symmetry on the unified direct exchange factor expression and the anisotropic nature of the scattering.

3. Results and discussion

The solutions to several benchmark problems are given in order to validate the DEF-based formulations presented here. The first two benchmark problems, however, deal exclusively with absorbing–emitting

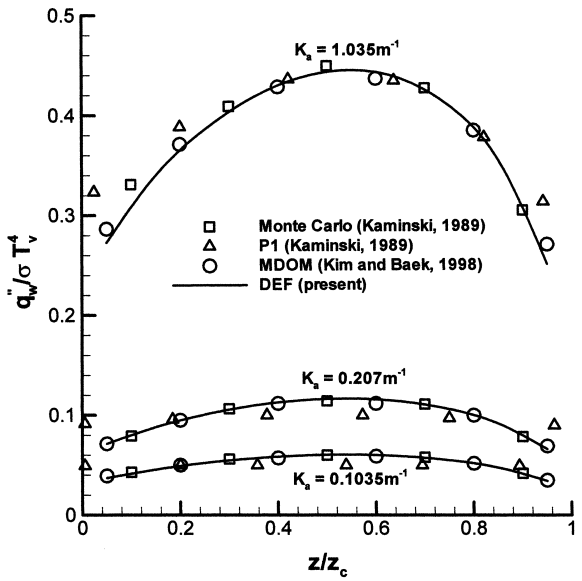

Fig. 3. Comparison of dimensionless wall heat flux distribution for a truncated cone using the source function, Monte Carlo, P1, and MDOM methods.

media in non-circular cylindrical enclosures. These cases are solved using the source function approach in an effort to illustrate the accuracy and flexibility of the DEF method in analyzing irregularly-shaped enclosures. The remaining cases presented in this section consider the effects of anisotropic scattering using the N-bounce and source function methods. All numerical simulations were performed on a 333 MHz Linux workstation with computational times of approximately 1952 and 6138 s for the one-bounce and source function methods, respectively, for a $10 \times 10 \times 10$ mesh.

The first benchmark problem considers a conical enclosure containing a hot absorbing–emitting medium, bounded by cold, black walls. The enclosure is of unit height, with radius/height ratios of $r_1/h = 0.0833$ at $z = 0$ and $r_2/h = 0.5833$ at $z = 1$. Fig. 3 presents the dimensionless wall heat flux distributions along the side-wall of the enclosure for $K_a = 0.1035$, 0.207 and 1.035 m^{-1} using the following solution techniques: P1 method [4], Monte Carlo method [4], MDOM [6], and source function method. The results obtained using the current method are in good agreement with the MDOM and Monte Carlo results for all values of the absorption coefficient. The P1 results, however, deviate from the results of the remaining methods at the bounding top/bottom surfaces for all optical conditions.

Next, the nozzle-shaped axisymmetric enclosure in the work of Kim and Baek [6] is examined. This enclosure, with an axial length, z_c, of 4 m, contains a hot, isothermal, absorbing–emitting medium with three different absorption coefficients, namely $K_a = 0.1$, 1.0 and 5.0 m^{-1}. The walls are, as in the previous problem, cold and black. The curved shape of the wall is generated from the following sinusoidal function:

$$\frac{r}{z_c} = \frac{1}{4}\left[1 + \sin\left(\frac{\pi z}{2z_c}\right)\right] \tag{23}$$

The dimensionless wall heat flux distributions obtained using the current method, the axisymmetric FVM, 3D-FVM, and MDOM, all from Kim and Baek [6], are shown in Fig. 4. These results are found to be in excellent agreement with each other for all absorption coefficients examined. Interestingly, the heat flux at the lower portion of the curved wall is approximately 10–15% higher than the heat flux near the top bounding surface. This can be attributed to the orientation of the ring elements on the wall at these locations relative to the cold, bounding top/bottom surfaces.

The problems examined up to this point consider non-scattering media only. The N-bounce and source function formulations can be implemented to solve problems with anisotropically scattering media. The accuracy of the N-bounce method, however, is user-designated and exhibits limited applicability. The term, N is practically limited to a value of 1 and is only good for low-to-moderate scattering, due to the non-linear increase in computational expense with increasing N. For cases where scattering is high, the source function approach produces results equivalent to an infinite bounce method at a significantly lower compu-

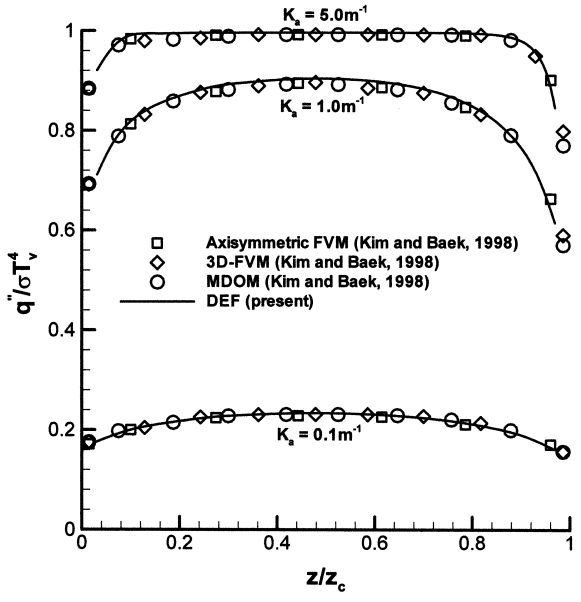

Fig. 4. Comparison of dimensionless wall heat flux distribution for a nozzle-shaped enclosure using the source function, axisymmetric FVM, 3D-FVM, and MDOM methods.

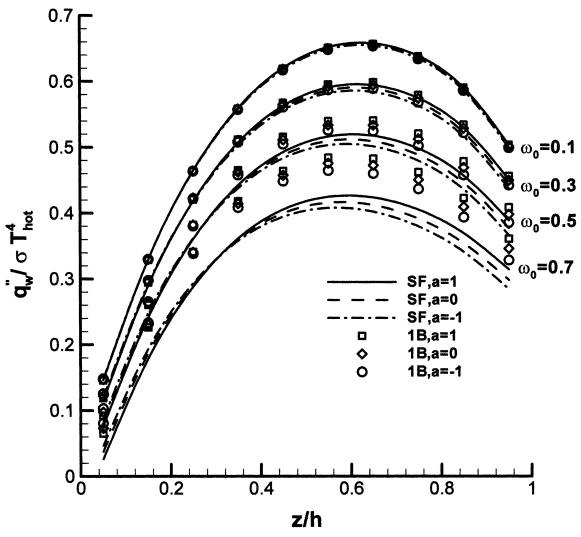

Fig. 5. Comparison of dimensionless wall heat flux distribution for a linear-anisotropically scattering cylindrical enclosure for $\omega_0 = 0.1$, 0.3, 0.5 and 0.7.

tational expense than that of the two-bounce method. To that end, consider a circular cylindrical enclosure of unit height and diameter encompassing a linear-anisotropically scattering medium. All surfaces are black. The phase function for this type of scattering can be expressed as:

$$\Phi(\Theta) = 1 + a\cos(\Theta) \tag{24}$$

where Θ is the scattering angle. The optical thickness of the medium, based on the diameter of the enclosure, is unity. The top of the enclosure (at $z = 1$) is cold; the bottom surface (at $z = 0$) is hot; the temperature of the wall and medium varies linearly between cold/hot temperatures. Fig. 5 gives a comparison of the wall heat flux distribution obtained using the source function and one-bounce methods for several selected values of scattering albedo. The results demonstrate that for low values of scattering albedo ($\omega_0 \leq 0.3$), the one-bounce and source function solutions are in good agreement, with a relative average percent error at each axial nodal point of approximately 0.1 and 1.3% for $\omega_0 =$ 0.1 and 0.3, respectively. As the scattering albedo increases further, the effects of the degree of anisotropy, namely, the value of a in Eq. (24), becomes more pronounced. Moreover, the one-bounce solution overpredicts the heat flux everywhere, yielding a relative average percent error of approximately 6.6% for $\omega_0 = 0.5$ and 24.7% for $\omega_0 = 0.7$. The relative average error for these cases is computed by evaluating the sum of the relative error, $|(q''_{1B} - q''_{SF})/q''_{SF}|$, for all nodes on the cylinder wall and dividing by N_z, the number of axial nodal points on the wall.

The radial distribution of dimensionless volume heat flux along $z/h = 0.5$ for several values of scattering albedo is given in Fig. 6. The figure shows, as in the previous case, the increasing disparity between the source function and one-bounce solutions for increasing scattering albedo. The approximate relative average percent errors for $\omega_0 = 0.1$, 0.3, 0.5 and 0.7 are 0.6%, 3.2%, 7.5% and 13.4%, respectively. These errors are, for the most part, greater than those reported for the surface heat flux results, with the exception of the $\omega_0 = 0.7$ case, where volumetric emission/absorption is now at a relatively low level.

Several cases of the aforementioned problem are additionally performed using $6 \times 6 \times 6$, $8 \times 8 \times 8$, $12 \times 12 \times 12$ and $14 \times 14 \times 14$ meshes to ensure grid-independence of the presented solutions. Fig. 7 gives a comparison of the dimensionless radiative wall flux obtained using the source function and one-bounce approaches for the $\omega_0 = 0.5$, $a = 1$ case. A comparison of total wall heat rate errors and computational times for the indicated cases is provided in Table 1. The $10 \times 10 \times 10$ mesh yields acceptable results for both one-bounce and source function methods, yielding a 6.5% and 1.1% error for the entire wall heat rate, respectively. The $12 \times 12 \times 12$ mesh would give better wall heat rate results for the one-bounce method (4.3%), but would require more computational effort and give results less accurate than those supplied by the $10 \times 10 \times 10$ source function approach.

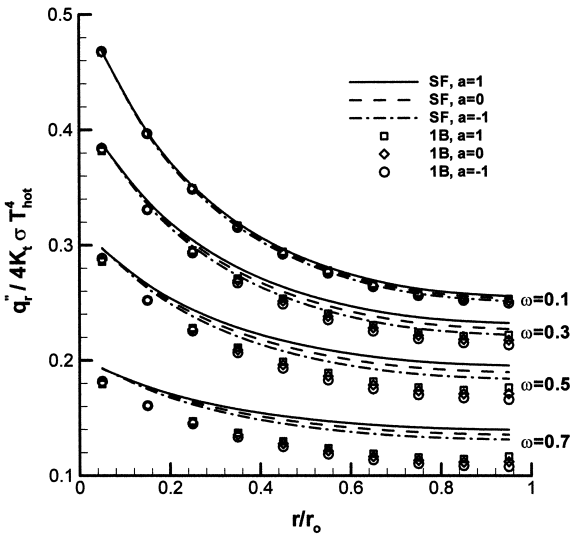

Fig. 6. Comparison of dimensionless volume heat flux distribution for a linear-anisotropically scattering cylindrical enclosure at $z/h = 0.5$ for $\omega_0 = 0.1$, 0.3, 0.5 and 0.7.

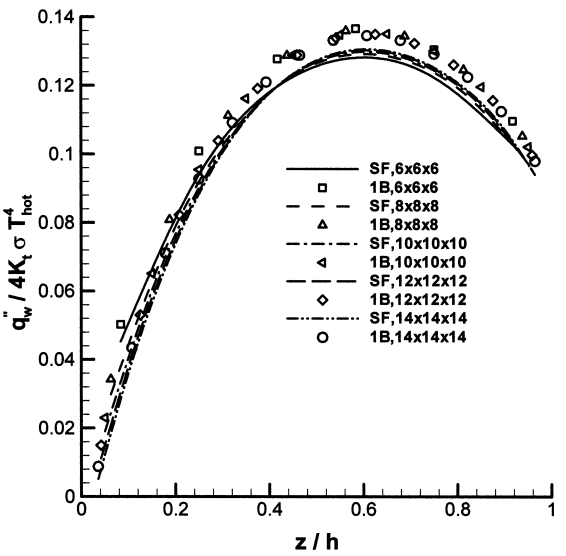

Fig. 7. Comparison of dimensionless wall heat flux distribution for a linear-anisotropically scattering cylindrical enclosure ($\omega_0 = 0.5$ and $a = 1$) for varying grid sizes.

Table 1
Comparison of total wall heat rate error and computation time on 333 MHz Linux workstation for a circular cylindrical enclosure

Mesh size	SF error (%)	1B error (%)	SF time (s)	10B time (s)
$6 \times 6 \times 6$	5.8	18.1	151	44
$8 \times 8 \times 8$	2.6	11.6	1278	394
$10 \times 10 \times 10$	1.1	6.5	6138	1952
$12 \times 12 \times 12$	0.4	4.3	27,126	8718
$14 \times 14 \times 14$	0.0	3.0	90,732	29,708

Next, consideration is given to axisymmetric enclosures with anisotropically scattering media. In the work of Azad and Modest [8], radiative transfer within an infinitely-long, black circular cylinder containing a linear anisotropically scattering medium is solved. The volume–surface temperature ratio is specified as 5:1; the scattering albedo is 0.5. This cylindrical system is modeled as a cylinder with a height–radius ratio of 5:1 using a $10 \times 13 \times 7$ ($N_r \times N_z \times N_\psi$) mesh, with top/bottom black enclosing surfaces prescribed at the medium temperature. Fig. 8 gives the dimensionless radial volumetric heat flux for varying degrees of anisotropy (value of a in Eq. (24)) and values of optical thickness (based on the radius of the cylindrical enclosure). To avoid crowding the graph, only the source function solution is depicted. The results display good agreement between both methods for all cases shown. Due to the low amount of absorbing/scattering present in the $\tau_0 = 0.2$ case, the radial heat flux is essential invariant to the type of anisotropic scatter.

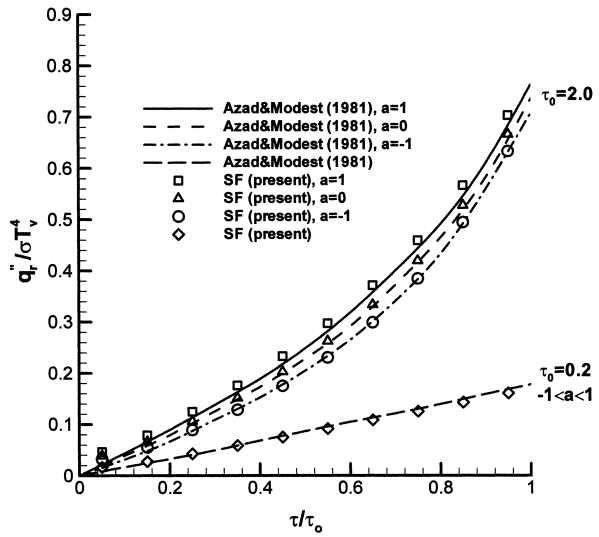

Fig. 8. Comparison of dimensionless radial heat flux distribution for a one-dimensional, linear-anisotropically scattering cylindrical enclosure using an exact formulation [8] and the source function method.

To this point, the path taken by a radiative beam within any of the aforementioned enclosures is completely unobstructed by the shape of the enclosure. There are, however, many cases of practical importance where the geometry of the enclosure produces shadowing (blockage) effects. For example, radiative analyses of high-pressure rocket nozzles are often very difficult to perform due to the complexities introduced by shadowing at the throat. Since there are no benchmark solutions for problems of this type, the solution of a rocket-nozzle problem is included to aid in benchmarking other axisymmetric formulations. Consider the rocket nozzle mesh layout (5×32) shown in Fig. 9. The radial/axial coordinates of the nozzle wall and surface/gas element temperatures are given in Table 2. The nozzle wall is gray, with an emissivity of 0.8; the top of the combustion chamber, perpendicular to the axis of the rocket nozzle, is black and at the temperature of the adjacent gas; the exiting cross-section has an emissivity of 0.8 and temperature equal to that of the neighboring gas. Since the objective of the current paper is to present a new model, radiative properties of the combustion products are appropriately defined. Therefore, the soot/carbon particles formed from com-

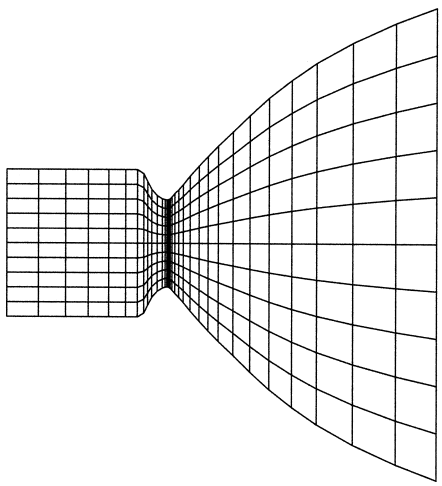

Fig. 9. Mesh layout of rocket engine.

bustion are assumed to have a particle diameter of 30 μm. The extinction and scattering coefficients for carbon particles of this size are obtained by using available spectral scattering/extinction efficiency data [14]. These coefficients are obtained by implementing the average integrated scattering/extinction efficiencies into the following equations:

$$K_t = \eta_t \frac{\pi D^2}{4} N \tag{25}$$

$$K_s = \eta_s \frac{\pi D^2}{4} N \tag{26}$$

where η_t and η_s are the extinction and scattering efficiencies; D is the diameter of the carbon particle; and N is the carbon particle concentration. The values of N chosen for purposes of investigation include $N = 5.0 \times 10^8$, 5.0×10^9, and 5.0×10^{10} (par/m^3). The δ-Eddington approximation is used to model the anisotropic scattering present within the enclosure.

Table 2
Nozzle radii and surface/gas temperatures along axial axis

z (cm)	r (cm)	T_s (K)	T_v (K)
−16.26	8.321	750.7	3834.8
−12.70	8.321	701.9	3834.8
−10.16	8.321	653.1	3834.8
−7.62	8.321	613.3	3834.8
−5.59	8.321	578.4	3834.8
−3.81	8.321	447.8	3834.8
−2.92	8.321	420.8	3834.8
−2.41	7.432	508.0	3830.7
−2.03	6.543	544.7	3821.6
−1.52	5.680	650.0	3797.5
−0.76	5.121	711.4	3746.4
−0.38	4.969	729.7	3704.8
−0.13	4.923	730.8	3665.8
0.00	4.918	686.1	3646.9
0.13	4.943	628.8	3605.6
0.25	5.019	521.2	3554.2
0.38	5.121	483.3	3502.1
0.64	5.426	461.6	3402.7
1.02	5.883	456.6	3295.4
1.52	6.289	454.2	3211.1
2.03	7.051	433.1	3098.4
3.05	8.220	384.1	2960.2
4.06	9.337	516.1	2851.7
5.08	10.404	502.4	2761.0
6.35	11.700	425.7	2664.2
8.38	13.579	510.8	2542.1
10.16	15.433	423.8	2433.1
12.70	17.542	439.4	2320.2
15.24	19.472	375.8	2228.4
18.29	21.402	333.4	2144.2
23.37	24.069	282.8	2042.3
27.94	25.847	238.4	1981.4

$$\Phi^*(\Theta) = 1 + 3g\cos(\Theta) \tag{27}$$

Since the δ-Eddington approximation removes the forward peak scattering from the scattering phase function and includes it in the extinction coefficient, the extinction and scattering coefficients are appropriately modified using the following equations:

$$K_t^* = K_t(1 - f\omega_0) \tag{28}$$

$$\omega_0^* = \frac{\omega_0(1-f)}{1 - f\omega_0} \tag{29}$$

where the values of f and g in the equations above are taken as $f = 0.111$ and $g = 0.215$ for moderate anisotropic scattering. Fig. 10 gives the dimensionless wall heat flux distribution along the rocket nozzle for the indicated particle concentrations using the isotropic DEF [1] source function and one-bounce methods. All the examined cases display similar trends for the wall flux. The sharp increase/decrease of heat flux between $z = -0.0381$ and $z = 0$ is due to enhanced/diminished visibility of the hot combustion products/surfaces in the combustor portion of the rocket nozzle. The results obtained for all three methods for the $N = 5.0 \times 10^8$ par/m^3 case are virtually identical due to the low amount of extinction present with the enclosure. The optical thickness, based on combustor radius, for this case is 0.146. For the $N = 5.0 \times 10^9$ par/m^3 case, the

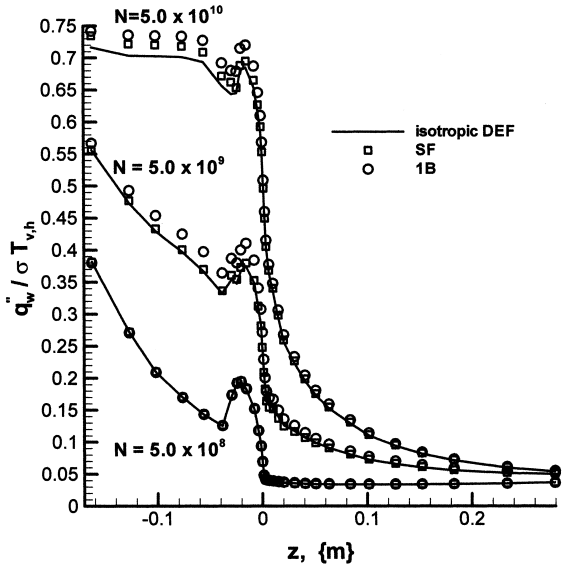

Fig. 10. Comparison of dimensionless wall heat flux profile in a rocket engine for particle concentrations of $N = 5 \times 10^8$, 5×10^9, and 5×10^{10} par/m^3.

source function and isotropic DEF solutions are relatively close, whereas the one-bounce solution is notably higher. The difference between the source function and isotropic DEF solutions becomes more pronounced in the last case, where the wall flux in the combustor region, computed by the source function method, is notably larger. Once again, the one-bounce method slightly overpredicts the heat flux along the combustor walls, due mainly to the relatively large scattering albedo of the medium ($\omega_0 = 0.537$).

4. Concluding remarks

The formulations for the source function and N-bounce variations of the DEF method are proposed for solving radiative transfer within irregularly-shaped axisymmetric enclosures containing an anisotropically scattering medium. The source function approach relates the surface/gas leaving intensities with the surface/volume emissive power and volumetric heat source. The method is iterative, versatile, and capable of handling all conditions of scattering. The N-bounce method is a multiple bounce method, where N, the maximum number of bounces a radiative beam makes before becoming completely absorbed, is user-defined. For a given mesh, the one-bounce solution requires substantially less computational time than the source function. The one-bounce method is, however, practically limited to problems with low-to-moderate scattering. Several benchmark problems are solved in order to validate the models, including radiative transfer within a truncated cone, nozzle-shaped enclosure, and infinitely-long cylinder. The results are found to be in excellent agreement with those in the literature. In addition, the solution to a rocket-nozzle problem with anisotropic scattering is presented to add to the benchmark literature.

Acknowledgements

This material is based upon work supported under a National Science Foundation Graduate Fellowship and by DARPA/AFOSR, as a part of The Consortium for Integrated Intelligent Modeling, Design, and Control of Crystal Growth Processes.

References

[1] E.M. Nunes, M.H.N. Naraghi, Numerical model for radiative heat transfer analysis in arbitrarily-shaped axisymmetric enclosures with gaseous media, Numerical Heat Transfer, Part A 103 (1998) 495–513.
[2] M.F. Modest, Radiative shape factors between differential ring elements on concentric axisymmetric bodies, AIAA Journal of Thermophysics and Heat Transfer 2 (1) (1988) 86–88.
[3] M.H.N. Naraghi, B.T.F. Chung, B. Litkouhi, A continuous exchange factor method for radiative exchange in enclosures with participating media, Journal of Heat Transfer 110 (2) (1988) 456–462.
[4] D.A. Kaminski, Radiative transfer from a gray, absorbing–emitting, isothermal medium in a conical enclosure, Journal of Solar Energy Engineering 111 (1989) 324–329.
[5] Z. Yin, Y. Jaluria, Zonal method to model radiative transport in an optical fiber drawing furnace, Journal of Heat Transfer 119 (1997) 597–603.
[6] M.Y. Kim, S.W. Baek, Radiative heat transfer in a body-fitted axisymmetric cylindrical enclosure, Journal of Thermophysics and Heat Transfer 12 (4) (1998) 596–599.
[7] L.W. Stockham, T.J. Love, Radiative heat transfer from a cylindrical cloud of particles, AIAA Journal 6 (10) (1968) 1935–1940.
[8] F.H. Azad, M.F. Modest, Evaluation of the radiative heat flux in absorbing, emitting and linear-anisotropically scattering cylindrical media, Journal of Heat Transfer 103 (1981) 350–356.
[9] S.T. Thynell, Effect of linear-anisotropic scattering on spectral emission from cylindrical plumes, Journal of Thermophysics and Heat Transfer 6 (2) (1992) 224–231.
[10] A.L. Crosbie, R.L. Dougherty, Two-dimensional radiative transfer in a cylindrical geometry with anisotropic scattering, Journal of Quantitative Spectroscopy and Radiative Transfer 25 (1981) 551–562.
[11] M.H.N. Naraghi, J. Huan, An N-bounce method for analysis of radiative transfer in enclosures with anisotropically scattering media, Journal of Heat Transfer 113 (3) (1991) 774–777.
[12] J. Huan, M.H.N. Naraghi, S.T. Thynell, J.R. Mahan (Eds.), Analysis of Radiative Heat Transfer in Three-Dimensional Absorbing, Emitting, and Scattering Media — A Source Function Approach, ASME HTD, vol. 154, 1990, pp. 357–369.
[13] M.E. Larsen, J.R. Howell, Least-squares smoothing of direct-exchange areas in zonal analysis, Journal of Heat Transfer 108 (1986) 239–242.
[14] P.J. Foster, C.R. Howarth, Optical constants of carbons and coals in the infrared, Carbon 6 (1968) 719–729.